

Spectroscopic Measurements of Bismuth

For Optical Diagnostics

David B. Scharfe* and Mark A. Cappelli†
Stanford University, Stanford, CA, 94305

Bismuth has received considerable attention recently as a propellant option for more advanced, next-generation Hall thrusters. A bismuth-fueled Hall thruster would possess advantages over conventional xenon thrusters in terms of efficiency, power-handling, and simplicity of ground testing facilities. In developing such a thruster, there is a need for non-intrusive diagnostic methods for taking the necessary measurements to optimize the geometry and operating conditions. A previous paper discussed such optical diagnostic methods for analyzing the velocity, energy, and number densities of BiI and BiII in the plume. Additionally, candidate transitions for measurement were selected and their lineshapes modeled in terms of hyperfine splitting and broadening mechanisms. In this paper, after a brief summary of the previous work, the line selections will be revised for improved accessibility to commercial tunable diode lasers. A lineshape model that more closely relates to Hall thruster measurements will also be discussed. Finally, the development of laboratory systems for taking measurements on a Bi gas will be discussed, and measurements of the Bi spectrum will be presented.

Nomenclature

A	= magnetic moment hyperfine splitting parameter
B	= quadrupole moment hyperfine splitting parameter
ΔE	= energy shift due to hyperfine splitting by nuclear spin
E	= energy between two electronic states
F	= total atomic angular momentum quantum number, including nuclear spin
I	= nuclear spin quantum number
J	= total atomic angular momentum quantum number, excluding nuclear spin
j	= single electron angular momentum quantum number
L	= total orbital angular momentum quantum number
$n \cdot L$	= species number density times absorption path length
λ, ν	= wavelength or frequency of light
n	= number density
S	= total electron spin angular momentum quantum number
T	= kinetic temperature
u	= bulk velocity (in direction of incoming laser beam)
ν_0	= linecenter frequency

* Research Assistant, Mechanical Engineering Department, Building 520. Member, AIAA.

† Professor, Mechanical Engineering Department, Building 520. Member, AIAA.

I. Introduction

Achieving the goal of faster missions to the outer planets requires significant improvements in the areas of spacecraft mass, efficiency, and flight time. The increase in velocity-increment required to significantly reduce the time of flight requires that either the propellant mass or the specific impulse (Isp) of the thruster be increased. Due to the dramatic cost increase associated with initially launching a larger-mass chemical rocket into Earth orbit, the method of choice for faster missions will lean toward high-Isp electric propulsion systems, like those flown on Deep Space I. However, state-of-the-art electric propulsion systems are still lacking in the efficiency and power handling required to effectively reduce flight time. Higher power Nuclear-Electric Propulsion (NEP) missions to the outer planets require a thruster capable of handling hundreds of kilowatts, while present ion engine technology is limited in power to less than 10kW.

In order to accommodate the requirements of future NEP missions, a bismuth-fueled two-stage Hall Thruster with Anode Layer (TAL) was selected as an option for further development[‡]. The proposed thruster would build on the TAL 160 and TAL 200 thrusters developed to operate on storable metal vapor propellants by TsNIMASH in Russia. A bismuth-fed Hall thruster offers significant advantages over ion thrusters; current TAL thrusters have been demonstrated to perform at 25-140kW and have the potential to scale up to greater than 500kW for future very high power NEP systems. Bismuth also offers several advantages over the xenon propellant used in current ion thrusters. Bismuth has a larger atomic mass, which serves to increase the thrust per particle for a rocket with a given Isp. Additionally, bismuth is condensable at room temperature, which allows for simpler testing on the ground in existing facilities as well as reduced spacecraft tankage fraction. Further, the ionization potential of bismuth is only 7.3eV, compared to 12.1eV for xenon, so that the propellant is more easily ionized and the thruster will have higher efficiency. Bismuth is also significantly less expensive and more readily available than is xenon.¹

In order to develop a Bi-fed Hall thruster, there will be a need for precise optimization of geometry and operating conditions, as well as accurate predictions of the potential for spacecraft contamination. This process will be contingent upon a characterization of the internal and near-field neutral bismuth (BiI) and bismuth ion (BiII) energy distribution, velocity field, and particle flux. A combination of laser-induced fluorescence (LIF) and absorption spectroscopy will be used to perform a portion of the necessary diagnostics.

This paper will summarize the previously-presented¹² analysis of the bismuth spectrum, and revise the previously discussed line selections. It is expected that LIF will be used to probe excited states in the BiI and BiII atomic and ionic particle stream to deduce the three-dimensional (3D) velocity (energy) distribution. While several electronic transitions of neutral and ionized bismuth are accessible with laboratory-laser systems (e.g., Ti-Sapphire or Ring-Dye lasers), they are not easily accessed with more compact laser sources that are more conveniently used in ground-test facilities suitable for thruster performance studies. The previous analysis and transition selections were based on accessibility to the New Focus brand Vortex line of lasers. However, these lasers have a limited tuning range of roughly 0.2nm in the IR and cannot capture certain transitions of bismuth due to the wide hyperfine splitting of this element and the Doppler shift corresponding to the 70km/s exhaust velocity expected for a 2-stage Bi thruster. Therefore, selections for the ions will be revised to make use of the New Focus brand Velocity line of diode lasers, which have a broader tuning range. Additionally, the previous work modeled the lineshapes of candidate transitions using Lorentzian and Doppler broadening assuming a shifted-Gaussian velocity distribution. This model will be revised to account for the more irregular velocity distribution predicted by a 2-D hybrid Hall thruster simulation developed at Stanford.

In addition to measurements of particle velocity, measurements of the number density of exhaust particles will be required for determining total particle fluxes. One possible option for ground state BiII number density will be the use of atomic resonance absorption spectroscopy of the 306.772nm ($6p^3 \ ^4S_{3/2} - 7s \ ^4P_{1/2}$) transition (vacuum wavelength: 306.86nm). For BiIII, a transition with the ground state as the lower state is located at 143.68nm ($6p^2 \ ^3P_0 - 7s \ ^3P_1$), which poses some difficulty as it is in the far vacuum-ultra-violet range.

Recent work has focused on the development of a means to measure features of interest in the bismuth spectrum prior to testing with a bismuth-fed thruster. A bismuth microwave discharge was described in the previous paper, but presented several difficulties. For the present work, a bismuth heat pipe apparatus has been developed; this device will be discussed and measurements of the Bi spectrum recorded in absorption and emission spectroscopy will be presented. In addition to further modification and measurement on the heat pipe, a laboratory Hall thruster is being modified to run on bismuth propellant for future analysis.

[‡] See, for example: http://www.aviationnow.com/content/ncof/ncf_n84.htm and press release: <http://quest.arc.nasa.gov/aero/news/08-30-02.txt>.

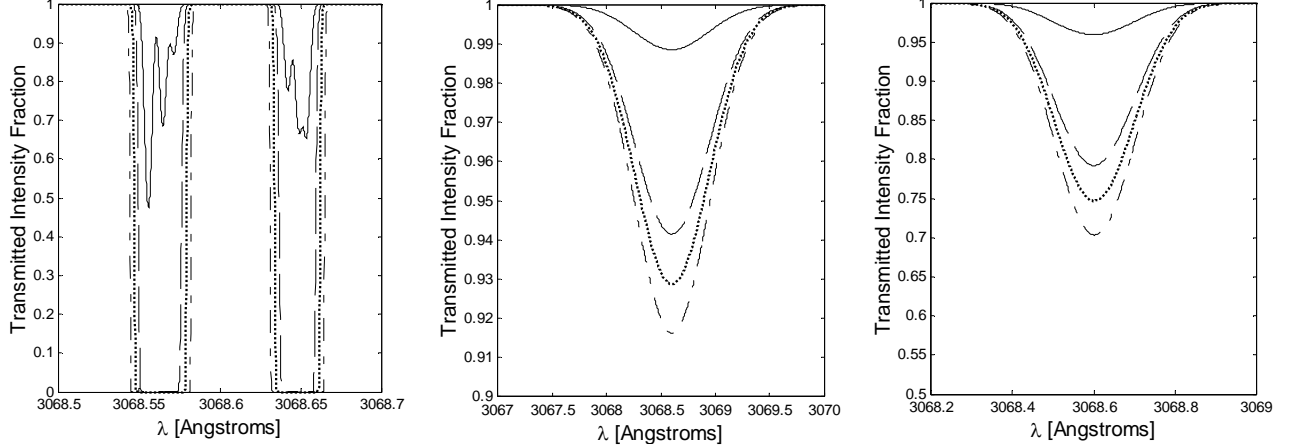


Figure 3: Absorption profiles for resonance transition of BiI with 1000K Doppler broadening. From left to right: true absorption profile, profile corresponding to 0.8Angstrom instrument resolution, and profile corresponding to 0.2Angstrom instrument resolution. In all plots: a solid line corresponds to $n\text{-}L$ product of $1 \times 10^{12} \text{ cm}^{-2}$, dashed line is $1 \times 10^{14} \text{ cm}^{-2}$, dotted line is $1 \times 10^{16} \text{ cm}^{-2}$, and dash-dotted line is $5 \times 10^{18} \text{ cm}^{-2}$.

where A and B are hyperfine splitting parameters for a given electronic state, and:

$$C = F(F + 1) - I(I + 1) - J(J + 1). \quad (3)$$

F is the angular momentum including nuclear spin and can take on multiple values according to:

$$F = J + I, J + I - 1, \dots, |J - I|, \quad (4)$$

where J is the total angular momentum (neglecting nuclear spin) for the electronic state considered. To predict the splitting of an electronic transition, the selection rule for transitions between the F -states of upper and lower electronic energy levels is:

$$\Delta F = 0, \pm 1, \quad (5)$$

but with $F = 0$ to $F = 0$ forbidden. Further, the relative intensity of each hyperfine-split transition component is determined by the so-called ‘‘sum rules’’ which relate the total intensity of lines going to and from a given F -state to the degeneracy of that state^{5,6,7}.

When measured in the laboratory, transitions will typically be broadened. The previous paper¹² discussed Doppler (assuming a Gaussian velocity distribution) and Lorentzian broadening mechanisms, and provided plots of a Voigt-profile which combines the effects of each.

Using these models, predicted absorption profiles were produced for the 307nm resonance transition of BiI, taking into account hyperfine splitting, broadening mechanisms, and using a simple moving average to approximate instrument resolution. Plots were produced for a variety of $n\text{-}L$ products (BiI number density times absorption path length), and are modified for the figure above, approximating the instrument response with a Gaussian curve.

III. Candidate Transition Refinement

The nature of the Bi spectrum, and the potentially high exhaust velocity of a 2-stage Bi Hall thruster (estimated at 70km/s), poses some additional difficulty in performing future LIF measurements. While the Vortex lasers discussed above can be configured for a wide range of specific wavelengths at the factory, once in the laboratory each laser can only scan a range of 60-80GHz (or roughly a maximum of 0.2nm near 800nm) about the factory-set central wavelength. It is noted here that the tentative LIF setup would require a single laser beam to be split to probe both the radial and axial velocities in the thruster plume simultaneously. The Doppler shift in transition frequency, $\delta\nu$, due to a mean velocity component, u , in the direction of the incoming laser beam, is given by:

$$\delta\nu = \nu_0 \frac{u}{c}, \quad (6)$$

where ν_0 is the unshifted linecenter frequency and c is the speed of light. For an axial velocity component of 70km/s probed by a laser of roughly 800nm, this corresponds to a shift of 87GHz, or roughly 0.2nm. Based on the Doppler shift alone, it would be quite difficult to probe the fast axial velocity and the slower moving radial velocity of a 2-stage thruster with a single Vortex laser. Further complicating matters, the 796nm line of BiII has a predicted hyperfine width of 0.18nm, and the BiII line at 853nm has a width of 0.11nm, making the task of scanning the entire shifted lineshape of a BiII transition for a variety of velocities up to 70km/s impossible with a single Vortex model laser.

Therefore, the next option will be to use the New Focus brand Velocity line of lasers for the ion lines. The Velocity TLB-6312 can scan from 765-781nm, and the Velocity TLB-6316 can scan 838-853nm. The only BiII lines within these ranges are located at wavelengths in air of 775.0nm and 838.8nm, as listed by NIST; there is also the possibility that the 6316 may be able to hit the BiII line at 853.2nm (these lines are at 775.2, 839.0, and 853.4nm, respectively, in vacuum).

However, analysis of these ion lines is not available in the literature, and they have not been absolutely assigned upper and lower electronic states. Taking the energy levels listed by Dolk and Moore, one can determine multiple possible upper and lower electronic state pairs for each. Matters are complicated by the fact that, as stated by Moore, bismuth is observed to undergo many forbidden transitions, so the use of selection rules can not be assumed to rule out possible transitions. Further, there is some disagreement between Moore and Dolk in terms of the precise energy, and even the existence, of some of the energetic electronic states of BiII. The possibilities for these transitions, based on all listed electronic states in the references, are summarized in the tables in the appendix. Based on a best-guess, we will assume here that the 775.2nm BiII transition is likely produced by the line calculated at 775.39nm from Dolk's energy states (775.31nm from Moore's data). The BiII line at 839.0nm is most likely produced by the transition calculated from Moore's tabulation, which also appears at 839.0nm. Dolk reports that transitions involving the upper electronic state (107976cm^{-1}) of this transition did not appear in his work. Further, Dolk's listing of energetic states does not provide any suitably close match to the 839.0nm line, so at this time there is no available hyperfine data for this transition. Finally, the 853.4nm line is given a new electronic transition assignment in this paper—it is more likely that this transition from NIST corresponds to the one at 853.02nm in Moore and 852.99nm in Dolk. However, we are again presented with a disagreement between the two references: a calculation from Moore reveals a likely transition at 853.46nm, but the upper electronic state (117004cm^{-1}) is again not listed by Dolk. The likely upper and lower electronic states for all of these transitions, along with hyperfine splitting constants, are listed in the table below. The resulting hyperfine split profiles are shown on the following page. Upon experimental measurement of these transitions, their corresponding energy levels and hyperfine splitting constants may be identified with more certainty from the recorded lineshapes.^{2,3}

Unfortunately, there are no BiI lines⁸ within the ranges that can be probed using the Velocity laser systems above. However, neutral Bi particles are not expected to be accelerated to the same high velocities as the ions. Additionally, the hyperfine splitting of BiI is relatively narrow when compared with that of the ion lines: the BiI line at 784nm is predicted to have a hyperfine split width of only 0.06nm, and the line at 854nm is expected to be split to roughly 0.02nm wide¹². These lines, therefore, may still be accessible to the less expensive Vortex class lasers from New Focus.

Table 1. Values of the Magnetic-Dipole A and Electric Quadrupole B coupling constants for select BiII states. Note that $1\text{mK} = 10^{-3}\text{cm}^{-1}$.^{2,3}

Energy Level [cm-1]	Designation	J	A [mK]	B [mK]
88566.685	6p7p(1/2,3/2)	1	-102.10	-1
88771.443	6p7s(3/2,1/2)	2	106	-38
88789.478	6p7p(1/2,3/2)	2	123.35	-12
96062.356	6s6p ³ D ₂	2	201.3	-9
101463.435	6p8s(1/2,1/2)	0	--	--
100494.931	6p6d(3/2,3/2)	1	108.4	11
105289.732	6p5f(1/2,7/2)	3	-28.8	-8
107976 (Moore)	³ P ₀	0	?	?
117004 (Moore)	³ F ₂ ?	2 ?	?	?

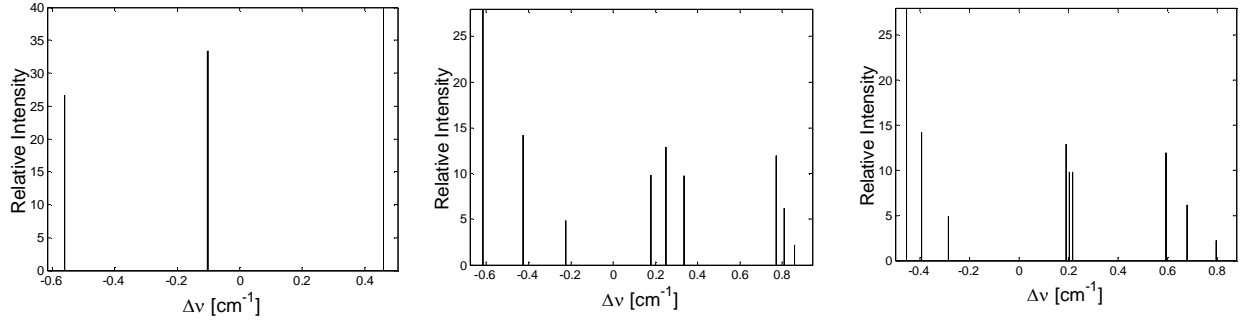


Figure 4. Hyperfine splitting profiles of BiII transitions. From left to right: 775.2nm transition, 853.4nm transition using old electronic state assignment, and 853.4nm transition using new assignment. Hyperfine splitting data for the 839.0nm transition is unavailable.

IV. Revised Lineshape Model

Previously, lineshapes were modeled assuming a shifted-Gaussian velocity distribution for ions and neutrals corresponding to various kinetic temperatures for the particles. However, collisions between fast-moving ions and slow neutrals can result in significant distortion to the velocity distribution – for ions, for example, this can result in a large group of fast moving particles that have not collided, and a smaller group of slow moving particles that have lost significant energy due to collisions. Additionally, for the ions, the velocity distribution cannot be expected to be Maxwellian even if collisions with other species are neglected. The velocity of a given ion would be determined by where it was ionized relative to the potential drop in the thruster channel. Therefore, rather than a thermal profile, the ion velocity distribution function would be based primarily on the distribution of the ionization zone relative to the spatially varying thruster potential. An example of this effect is illustrated in the figure below for the 775 and 853nm transitions. The ion velocity distribution used here is taken from the exit plane in a 2-D hybrid Hall thruster simulation developed at Stanford University. Note that the broadened profiles of each line clearly show the result of the hyperfine structure – these profiles are in the range of 0.1-0.15nm wide and should be resolvable with a tunable laser source. Typical thruster measurements on xenon do not generally show the effects of its comparatively narrow hyperfine splitting⁷. Additionally, the width of these lines evidences the need for lineshape models before attempting diagnostic measurements, as discussed above with regard to selecting appropriate New Focus lasers.

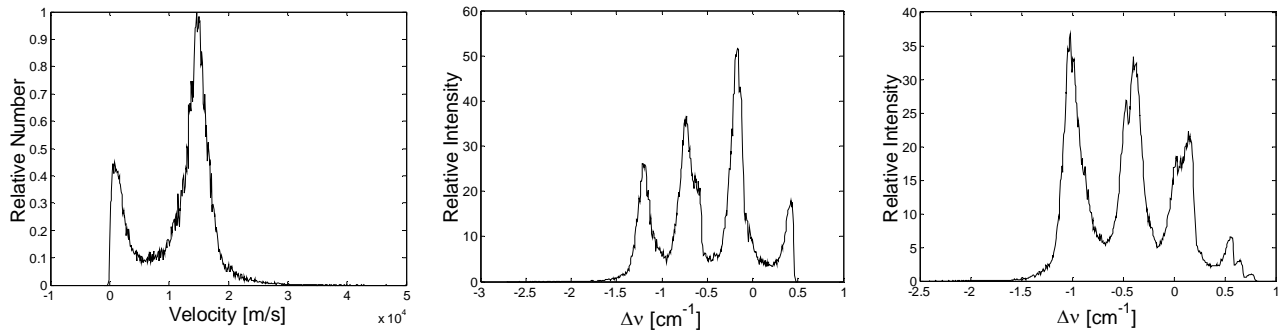


Figure 5. Simulated velocity distribution and resulting Doppler broadening of BiII lines. From left to right: Velocity distribution calculated at exit plane of simulated thruster, broadening of 775nm line, and broadening of 853nm line of BiII.

V. Measurements of Bi Spectrum

A bismuth heat pipe apparatus, based on the design of Cappelli, et. al.^{10,11}, has been developed in order to measure and further analyze the Bi spectrum before putting the diagnostics to use on an actual thruster. The apparatus consists of an electrically heated metal mesh inside a small vacuum chamber. Bismuth is placed onto the center of the mesh, and the outer edges of the mesh are cooled so that the vaporized bismuth will condense out and wick back toward the hot center. Argon is pumped into the chamber to help contain the bismuth in the cavity and prevent it from plating out onto the walls and windows. Additionally, a pair of electrodes inside the chamber is used to generate a hollow cathode discharge that produces light-emitting Bi plasma. The electrodes are typically run at 600V with current on the order of 1mA. A deuterium lamp outside the chamber is used as a broad light source for

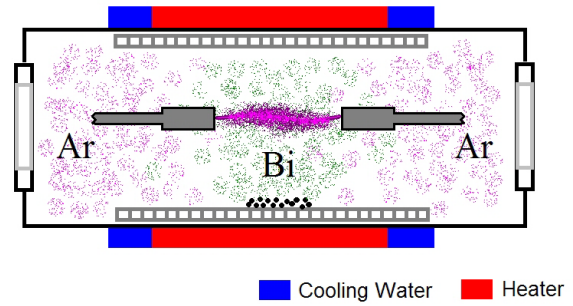
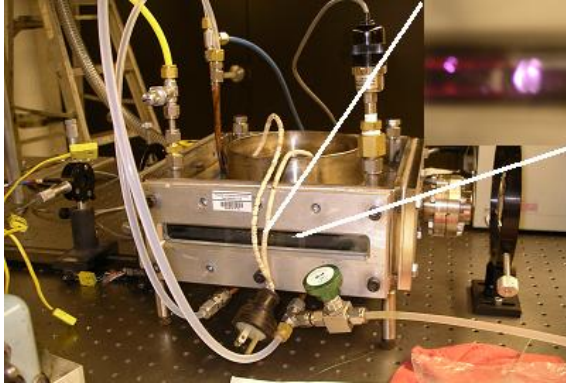


Figure 6. Bismuth Heat Pipe apparatus.

absorption analysis near the BiI resonance transition. A thermocouple between the electrical heater and the heat pipe mesh is used to estimate the temperature (and therefore the vapor pressure) of the Bi inside the chamber. Data was recorded using a 1/2m monochromator and a Hamamatsu R928 photo-multiplier tube (PMT). The exit and entrance slits of the monochromator were held at 10micrometers for absorption scans, and 40micrometers for emission measurements. The signal from the PMT was passed to a Stanford Research SR850 Lock-in Amplifier

Thus far, the heat pipe has been used to successfully record both absorption and emission from the 307nm resonance transition of neutral bismuth. Sample scans, with absorption measurements at various thermocouple temperatures, are shown in the figure below. Note that as the chamber is cooled, the absorption disappears because the vapor pressure of the bismuth is decreasing; this verifies that the line observed is indeed bismuth. Similar results were seen for emission scans. However, after heating the chamber for an extended period and then cooling it, the bismuth line would still appear in the emitted light, indicating that perhaps an amount of bismuth had plated out onto the electrodes and was being re-vaporized without the need for the electrical heaters.

A simple analysis of the peak absorbed fraction of light can be used to estimate the $n-L$ product discussed earlier in this paper. Based on the width of the absorption profile in the figure below, and analysis for various instrument resolutions as illustrated in Figure 3, it is estimated that the instrument resolution for these trials corresponds to roughly 0.8Angstroms in modeled profiles. Comparing to the data in Figure 3, and estimating an absorption path length of 10cm inside the cell, the peak absorption fraction at each temperature can be used to estimate the vapor pressure, and therefore the temperature, of the bismuth in the cell. For example, at 850°C, the absorbed fraction was roughly 7.2%. This would correspond to an $n-L$ product of roughly $1 \times 10^{16} \text{cm}^{-2}$, and therefore a number density of $1 \times 10^{15} \text{cm}^{-3}$. At roughly 1000K, this would correspond to a bismuth pressure on the order of 100millitorr; this vapor pressure corresponds to a bismuth temperature closer to 800°C, providing an estimate of the temperature drop between the thermocouple and the inside of the heated mesh. However, a more precise analysis, requiring iteration of the temperature (used in Doppler broadening of the transition and calculating pressure from number density), a more accurate determination of the instrument resolution (FWHM of Gaussian response curve), and an averaging of multiple measurements to reduce signal noise, would be necessary to make calculations beyond order-of-magnitude. What is more important here is that as the temperature was reduced, the corresponding drop in bismuth number density was observable in a qualitative sense in the absorption profiles. This type of relative analysis will be important in analyzing a thruster, where precise species temperatures for Doppler broadened transitions may not be instantaneously available for an exact analysis.

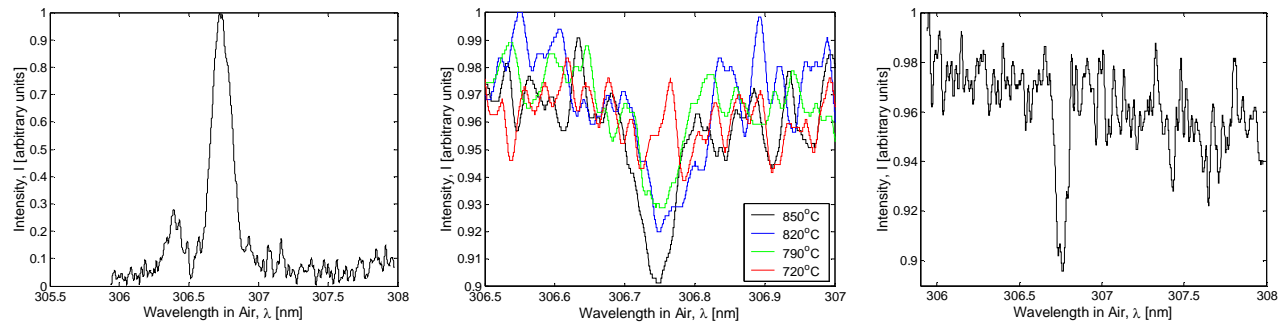


Figure 7. Measurements of the BiI resonance line in heat pipe chamber. From left to right: emission, absorption at various temperatures (decreased with time), and absorption at 850°C again to show consistency over time.

Although the 307nm line was observed consistently in both absorption and emission, at the present time, none of the other candidate transitions can be observed in the emission spectrum from the heat pipe cavity. It is thought that the discharge is too weak to produce a significant population in the highly excited upper states of these transitions, and some modification to the setup is necessary.

VI. Conclusion

As work continues on this project, advancement of the diagnostics will be continued by increased modification to the heat pipe cavity. The geometry and operating conditions of the electrodes will be redesigned to produce a stronger discharge that should provide a better tool for measuring excited states of BiI and BiII and analyzing the candidate transitions. Additionally, work is currently being performed to modify laboratory model hall thrusters to run on a Bi propellant for analysis of high velocity bismuth plasma.

Appendix

Appendix Table 1. Possible transitions corresponding to the 775.2, 839.0, and 853.4nm lines of BiII, using the energy level data from Moore. Allowed transitions are determined here from the requirement that $\Delta S = 0$, $\Delta L = +1$ or -1 , and $\Delta J = 0, +1, \text{ or } -1$ in the term symbol $^{2S+1}L_J$. Wavelengths noted with a * are those expected to correspond with the candidate transitions. A ** indicates the previously used assignment¹², and * indicates a transition that would be used, except that one of the states is missing in Dolk so hyperfine data cannot be determined.^{2,3,9}**

Vacuum Wavelength [nm]	Lower Level		Upper Level		Forbidden Transition?	States Also Listed in Dolk?
	Energy [cm ⁻¹]	Term Symbol	Energy [cm ⁻¹]	Term Symbol		
774.35	69133	³ P ₀	82047	³ F ₂	Forbidden (L, J)	Lower and Upper
776.34	82047	³ F ₂	94928	³ D ₂	Allowed	Lower and Upper
775.31*	88566	¹ P ₁	101464	³ P ₀	Forbidden (S, L)	Lower and Upper
773.40	103003	³ D ₃	115933	³ G ₃	Forbidden (L)	Lower and Upper
838.01	87078	³ P ₀	99011	³ P ₂	Forbidden (J, L)	Lower and Upper
838.50	88566	¹ P ₁	100492	³ P ₁	Forbidden (S, L)	Lower and Upper
839.00*	96057	³ D ₃	107976	³ P ₀	Forbidden (J)	Lower only
836.82	96057	³ D ₃	108007	¹ F ₃	Forbidden (S)	Lower and Upper
838.86	105083	³ F ₂	117004	³ F ₂ ?	Forbidden (L)	Lower only
853.02*	88769	³ P ₂	100492	³ P ₁	Forbidden (L)	Lower and Upper
854.48**	88789	³ D ₂	100492	³ P ₁	Allowed	Lower and Upper
852.15	105269	³ P ₂	117004	³ F ₂ ?	Forbidden (L)	Lower only, but listed with J=1
853.46***	105287	³ G ₃	117004	³ F ₂ ?	Allowed	Lower only

Appendix Table 2. Possible transitions corresponding to the 775.2, 839.0, and 853.4nm lines of BiIII, using the energy level data from Dolk. Allowed transitions are determined here from the specific (j,j)-coupling selection rule that for the electron making a jump, $\Delta j = 0, +1, \text{ or } -1$ ⁹. Wavelengths noted with a * are those expected to correspond with the candidate transitions; ** was previously used¹². A * indicates a transition predicted in Moore that would be used, except that one of the states is missing in Dolk so hyperfine data cannot be determined.^{2,3,9}**

Vacuum Wavelength [nm]	Lower Level			Upper Level			Forbidden Transition?
	Energy [cm ⁻¹]	Designation	J	Energy [cm ⁻¹]	Designation	J	
774.25	69133.891	6p7s(1/2,1/2)	0	82049.632	6p6d(1/2,5/2)	2	(j,j) Forbidden
776.34	82049.632	6p6d(1/2,5/2)	2	94930.640	6s6p ³ D ₂	2	
775.39*	88566.685	6p7p(1/2,3/2)	1	101463.44	6p8s(1/2,1/2)	0	(j,j) Allowed
773.21	103003.505	6p6d(3/2,3/2)	3	115936.556	6p6f(1/2,5/2)	3	
776.06	112650.875	6p7p(3/2,3/2)	0	125536.550	6p5f(3/2,7/2)	4	(j,j) Forbidden
838.04	87078.777	6p7p(1/2,1/2)	0	99011.328	6p6d(3/2,5/2)	2	
838.35	88566.685	6p7p(1/2,3/2)	1	100494.931	6p6d(3/2,3/2)	1	(j,j) Allowed
837.88	105289.732	6p5f(1/2,7/2)	3	117224.556	6p8d(1/2,5/2)	3	(j,j) Allowed
852.99*	88771.443	6p7s(3/2,1/2)	2	100494.931	6p6d(3/2,3/2)	1	(j,j) Allowed
854.30**	88789.478	6p7p(1/2,3/2)	2	100494.931	6p6d(3/2,3/2)	1	(j,j) Allowed
854.89	105527.197	6p6d(1/2,3/2)	2	117224.556	6p8d(1/2,5/2)	3	(j,j) Allowed
839.0***	96062.356	6s6p ³ D ₃	3	107976			
853.46***	105289.732	6p5f(1/2,7/2)	3	117004			

Acknowledgments

This research was supported in part by the Air Force Office of Scientific Research and by the National Aeronautics and Space Administration. Stipend support for D. Scharfe was provided through a fellowship from the Department of Defense/ASEE.

References

- ¹Tverdokhlebov, S., Semenkin, A., and Polk, J., "Bismuth Propellant Option for Very High Power TAL Thruster," 40th AIAA Aerospace Sciences Meeting & Exhibit, AIAA, 14-17 January 2002.
- ²Moore, C.E., *Atomic Energy Levels as Derived From the Analyses of Optical Spectra*, Volume III, National Bureau of Standards, Circular 467, U.S. Government Printing Office, Washington, D.C., 1958, May 1, 1958, pp219-222.
- ³Dolk, L., Litzen, U., and Wahlgren, G.M., "The Laboratory Analysis of Bi II and its Application to the Bi-rich HgMn Star HR 7775," *Astronomy & Astrophysics* 388, 2002, pp. 692-703.
- ⁴George, S., Munsee, J.H. and Vergès, J., "Hyperfine-structure Measurements in Bismuth Using a Fourier-transform Spectrometer" *J. Opt. Soc. Am. B*/Vol. 2, No. 8, August 1985, pp. 1258-1263.
- ⁵Sobelman, I.I., *Atomic Spectra and Radiative Transitions*, 2nd ed., Springer-Verlag, New York, 1992, p. 170.
- ⁶H.G. Kuhn, F.R.S., *Atomic Spectra*, Academic Press, New York, 1969, p.191.
- ⁷Cedolin, R.J., *Laser-Induced Fluorescence Diagnostics of Xenon Plasmas*, Report No. TSD-105, Ph.D. Dissertation, High Temperature Gasdynamics Laboratory, Mechanical Engineering Dept., Stanford University, Stanford, CA, June 1997, p. 56..
- ⁸NIST Atomic Spectra Database Lines Form, http://physics.nist.gov/cgi-bin/AtData/lines_form.
- ⁹Herzberg, Gerhard. *Atomic Spectra and Atomic Structure*, Dover Publications, New York, 1944, p.154.
- ¹⁰Cappelli, M.A., M.A.Sc. Thesis, U. Toronto, Institute for Aerospace Studies (1983).
- ¹¹Cappelli, M.A., Cardinal P.G., Herchen, H., and Measures, R.M., "Sodium atom distribution within a heat sandwich oven," *Rev. Sci. Instrum.* 56 (11), November 1985, pp. 2030-2037.
- ¹²Scharfe, D.B., and Cappelli, M.A., "Optical Diagnostic Options for Bismuth Hall Thrusters," AIAA-2004-3946, 40th AIAA/ASME/ASEE Joint Propulsion Conference, AIAA, 11-14 July 2004.